Length scale control for high-resolution three-dimensional level set–based topology optimization

Aage, Niels; Giele, Reinier; Andreasen, Casper Schousboe

Published in:
Structural and Multidisciplinary Optimization

Link to article, DOI:
10.1007/s00158-021-02904-4

Publication date:
2021

Document Version
Peer reviewed version

Noname manuscript No.
(will be inserted by the editor)

Length scale control for high resolution three dimensional level set based topology optimization

Niels Aage · Reinier Giele · Casper Schousboe Andreasen

Received: date / Accepted: date

Abstract This work considers an efficient approach for length scale control in high resolution three-dimensional level set based topology optimization. A contrast parameter based cut element method is employed to ensure a crisp interface representation while working on fixed background hexahedral meshes. This enables the use of efficient multigrid preconditioned Krylov methods in massively parallelized computations. The minimum length scale is controlled using a projection filter without the need for β-continuation. The capabilities of the proposed approach is demonstrated on several numerical examples using more than 62 million hexahedral elements.

Keywords Topology optimization · Large-scale · Level set method · Cut elements · Length scale control

1 Introduction

Since its introduction in the late 1980's, the density based topology optimization method (Bendsøe and Kikuchi, 1988; Bendsøe, 1989) has proven to be an indispensable tool in the pursuit of novel designs in both academia and industry. The main reasons for the success of the density method, is due to the existence of fast and robust solution methods, including efficient gradient based optimizers, length scale control schemes, carefully tailored linear solvers and freely available open source codes. Besides the standard density based method, several alternative topology optimization approaches exist including moving morphable components, phase field methods, (de-)homogenization approaches, evolutionary methods, level set methods, etc. and the reader is referred to e.g Bendsøe and Sigmund (2004); Sigmund and Maute (2013) for a comparative review.

This work proposes a crisp interface level set method (Osher and Sethian, 1988; Sethian and Wiegmann, 2000) capable of solving large-scale problems through high-performance computing (Evgrafov et al., 2008; Amir et al., 2014; Aage et al., 2015, 2017; Liu et al., 2019a; Baandrup et al., 2020) with control of the minimum length scale. The combination of high resolution designs and length scale control is crucial to make any topology optimization method industrially relevant. However, for level set methods the construction of a large-scale capable numerical scheme poses a number of challenges due to the following considerations. For example, if remeshing is employed to ensure the crisp interface, e.g. (Dapogny et al., 2014; Feppon et al., 2021), the load balancing will have to be recomputed between design cycles which, together with the remeshing itself, reduces the performance of the numerical approach. The remeshing can be partly alleviated by utilizing immersed boundary methods such as CutFEM (Hansbo and Hansbo, 2004; Burman, 2010). Although CutFEM does not enrich the solution space as done in e.g. XFEM (Belytschko and Black, 1999), the ficticious domain mesh is still truncated close to the interface, which in turn means that the degrees of freedom (dofs) must be renumbered at

N. Aage
Department of Mechanical Engineering, Section for Solid Mechanics, Technical University of Denmark, Nils Koppels Allé, Building 404, DK-2800 Kgs. Lyngby, Denmark
E-mail: naage@mek.dtu.dk

R. Giele
Department of Precision and Microsystems Engineering, Section for Solid Mechanics, Delft University of Technology, Mekelweg 2, 2628 CD Delft, The Netherlands

C. S. Andreasen
Department of Mechanical Engineering, Section for Solid Mechanics, Technical University of Denmark, Nils Koppels Allé, Building 404, DK-2800 Kgs. Lyngby, Denmark

every design iteration which again reduces the parallel performance. We remark, that renumbering of dofs does not pose a significant problem for pure analyses, and that efficient preconditioners for such problems are currently receiving much attention see e.g. de Prenter et al. (2020). Hence, the motivation for this work is to demonstrate that crisp interface level set methods can be used for the efficient solution of large-scale topology optimization problems with an imposed length-scale.

Imposing a predefined length scale in level set methods have previously been studied using energy methods (Chen et al., 2008), by explicit distance penalization (Dapogny et al., 2017) and through a fictitious model problem (Yamada, 2019). In Chen et al. (2010) and Chen and Chen (2011) the authors study uncertainties in load-conditions as well as uncertainties associated with random boundary variations. Other approaches build directly on methods originally developed for density methods. An example is the geometric constraints by Zhou et al. (2015) which is used for level set problems in Jansen (2019). In this study the length scale control is imposed using the three-field robust design approach from density methods (Bourdin, 2001; Wang et al., 2011), and hence, this work is a direct extension of the approach from Andreasen et al. (2020) to three dimensions. Turning to large-scale methods for high resolution level set based optimization, the number of publications is noticeable low although some recent studies can be found e.g. Barrera et al. (2020); Feppon et al. (2020). The fact is that careful tailoring of numerical methods for very high resolution topology optimization level set approaches has not received the same amount of attention as seen for density methods. This could, however, be changing as recent publications (Liu et al., 2019b; Kambampati et al., 2020) have shown how solution methods originally designed for density methods (Amir et al., 2014; Aage et al., 2015), also allows for efficient level set methods. Likewise, in this work we adopt a multigrid preconditioned Krylov method to enable high resolution designs.

In summary, the main contributions of this work are 1) a design methodology capable of introducing length scale control for 3D level set problems. This has, to the best of the authors' knowledge, not been shown before for 3D level set approaches and 2) to demonstrate that the linear systems arising from crisp interface level set methods can be solved efficiently using multigrid preconditioned Krylov solvers developed for density methods.

The rest of the paper is organized as follows. Section 2 presents the problem formulation and the length scale control scheme, followed by a brief introduction to the cut element method with emphasis on large-scale modeling challenges. In section 3 the capabilities of the design method is demonstrated on two minimum compliance design problems using more than 60 million elements. Finally, the findings are summarized and discussed in section 4.

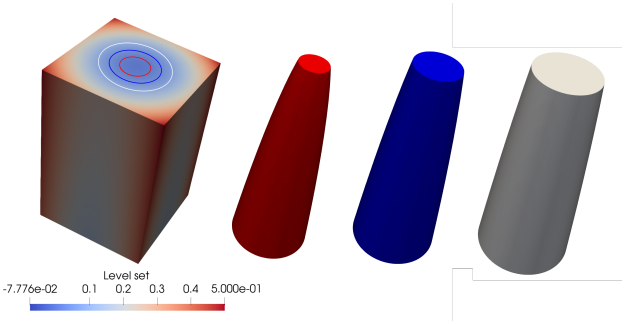

Fig. 1: Illustration of the robust design approach. The rectangular domain to the left is colored by its level set values and the thresholded realizations are from left to right: eroded (red), blueprint (blue) and dilated (gray).

2 Problem formulation

This work considers three-dimensional minimum compliance problems following the level set approach presented in Andreasen et al. (2020). The minimum length scale is controlled through the simplified robust approach (Wang et al., 2011) in which the design formalism operates with three realizations, i.e. a blueprint, a dilated and an eroded design, c.f. the illustration shown in Figure 1. The simplified robust approach utilizes the fact that, assuming the topology does not change, the compliance is always largest for the eroded design and that the volume is always largest for the dilated design. Hence, the resulting optimization problem can be formulated as

$$\begin{aligned} \min_{\boldsymbol{s}\in\mathbb{R}^n} : \quad & \Phi = [\mathbf{u}^e]^T \mathbf{K}^e \mathbf{u}^e \\ \text{subject to:} \quad & \mathbf{K}^e(\mathbf{s})\mathbf{u}^e = \mathbf{f} \\ & V^d(\mathbf{s})/V^* - 1 \leq 0 \\ & 0 \leq s_i \leq 1, \quad \forall i \end{aligned} \tag{1}$$

where $\mathbf{s}$ is a vector of nodal design variables, $\mathbf{u}^e$ and $\mathbf{K}^e$ refer to the displacement field and stiffness matrix, respectively, in which $(\cdot)^e$ denotes the eroded realization and $\mathbf{f}$ refers to the load vector. The linear elasticity problem is solved on a fixed, structured hexahedral background mesh and only for the eroded realization, i.e. $\mathbf{K}^e(\mathbf{s})\mathbf{u}^e = \mathbf{f}$. Similarly, the objective function is also evaluated for the eroded design $[\mathbf{u}^e]^T \mathbf{K}^e \mathbf{u}^e$. The volume constraint is imposed on the dilated design with

volume fraction $V^d(\mathbf{s})$. To ensure that the optimized design meets the target volume fraction for the blueprint design, the volume fraction V^* is updated at every 20th iteration as $V^* = \frac{V^d(\mathbf{s})}{V^b(\mathbf{s})} V^b_{\text{target}}$, where $V^b(\mathbf{s})$ refers to the blueprint volume fraction. Finally, a box constraint is included to bound the design variables between 0 and 1.

The optimization problem is solved using a parallelized version of the Method of Moving Asymptotes (MMA) (Aage and Lazarov, 2013; Svanberg, 1987) for which the sensitivities are obtained using the semi-discrete adjoint approach (Sharma et al., 2017).

2.1 Level set parametrization and length scale control

The design parametrization used in this work is identical to that presented in Andreasen et al. (2020), and is summarized here for completeness only.

The physical level set field needed for the cut element modeling approach is obtained through a projection filter based on the three-field robust formulation from Wang et al. (2011). The first step is to apply a smoothing filter on the mathematical design variables, i.e.

$$\tilde{s}_i = \frac{\sum_{j \in N_{i,j}} s_j w(\boldsymbol{x}_j)}{\sum_{j \in N_{i,j}} w(\boldsymbol{x}_j)} \tag{2}$$

where $N_{i,j}$ is the neighborhood set defined by $w(\boldsymbol{x}_j) = R - |\boldsymbol{x}_j - \boldsymbol{x}_i|$ with R being the radius of influence. Next, the filtered field is projected using a smooth Heaviside function as

$$\hat{\boldsymbol{s}} = \frac{\tanh(\beta\eta^k) + \tanh(\beta(\tilde{\boldsymbol{s}} - \eta^k))}{\tanh(\beta\eta^k) + \tanh(\beta(1 - \eta^k))} \tag{3}$$

where $\beta = 12$ is the steepness parameter and η^k controls the threshold location which takes on different values for the dilated, blueprint and eroded realizations, i.e. $k = \{d, b, e\}$. Throughout this work a uniform offset, $\Delta\eta$, is used such that $\eta_e = \eta_b + \Delta\eta$ and $\eta_d = \eta_b - \Delta\eta$. To ensure that the design update is robust wrt. mesh refinement, i.e. changing the size of the finite elements, the final step is to perform a mapping such that the physical level set field takes on values between $\pm h/2$ where h is the element side length, i.e.

$$\bar{\hat{\boldsymbol{s}}} = h\left(\hat{\boldsymbol{s}} - \frac{1}{2}\right) \tag{4}$$

It is worth to remark that the level set adaptation of the robust approach from density methods does not rely on a β-continuation scheme. Also note that in order to predict the exact length scale imposed by the robust approach following the analytical expressions from Wang et al. (2011), one would need to let $\beta \to \infty$. However, for the presented level set approach the steepness is set rather low in order to avoid stair casing, i.e. non-smooth interfaces in the optimized designs. Moreover, based on extensive numerical studies in both 2D and 3D it is found that the combination of a relatively large filter radius and $\beta = 12$ results in an easily identifiable and easily controllable length scales in the optimized design. If exact control of the length scale is paramount, while still maintaining the smooth edges, one could most likely apply the double filter proposed in Christiansen et al. (2015).

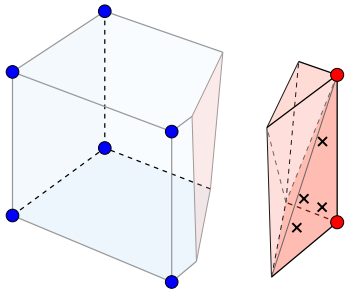

Fig. 2: Illustration of a single hexahedral cut element split into two phases, namely void (blue) and solid (red). The solid part to the right is tetrahedralized into two sub tetrahedrals and for one of them its local Gauss points are shown in the coordinate system of the parent hexahedral.

2.2 Cut element method

This section compactly presents the utilized cut element method such that only the core of the scheme is introduced. Again, the reader is referred to Andreasen et al. (2020) for details and the following is focused on any noticeable differences when going into three dimensions.

The cut locations are determined based on the physical level set field such that $\bar{\hat{s}}_i > 0$ corresponds to solid, $\bar{\hat{s}}_i < 0$ to void and $\bar{\hat{s}}_i = 0$ to the interface. Working on a fixed, structured hexahedral background mesh, the interface is realized using the marching cubes algorithm (Lorensen and Cline, 1987). After the cut locations have been identified, the resulting polyhedrons are assigned a material phase, i.e. either solid or void, and subsequently tetrahedralized using TetGen (Si, 2015) as shown in Figure 2.

The core of the cut element method is to map the Gauss points from each of the sub-tetrahedrals back to the parent hexahedral local coordinates, to compute the volume ratio of tetrahedral sub-element to hexahe-

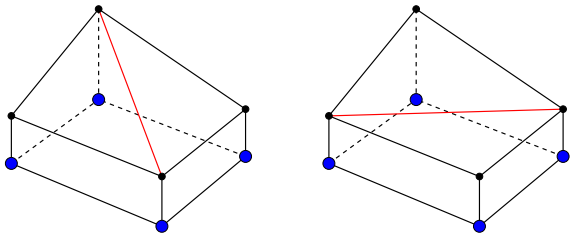

Fig. 3: Ambiguous cut configuration on a surface.

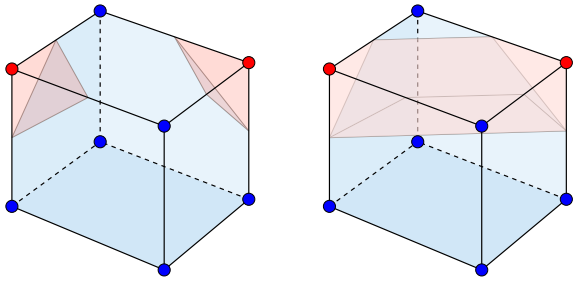

Fig. 4: Ambiguous cut configuration on the interior.

dral parent-element, and then to perform the numerical (over-)integration using quadrature. Contrary to many XFEM (Belytschko and Black, 1999) or CutFEM (Hansbo and Hansbo, 2004) approaches, we assign an artificial stiffness to the void region, $E_{\min} = 10^{-7}E_0$, where E_0 refers to the elastic modulus of the base material. Equally important is it that the integration is performed in the full modeling domain and not just in the solid region including the cut elements. Despite the introduction of additional degrees of freedom, such an approach is very well suited for parallel computations as the background mesh remains constant throughout the design process, and hence, the work balance can be kept constant throughout the optimization process. Furthermore, the inclusion of a contrast parameter alleviates the need for stabilization such as ghost penalties (Burman, 2010).

It is, however, important to realize that the combination of a hexahedral background mesh and cuts realized by sub-tetrahedrals can lead to several ambiguous configurations that must be handled correctly (Barrera and Maute, 2020). For example, when four edges of the hexahedral are cut, the resulting surface can be triangulated in two distinct ways as shown in Figure 3. Similarly, if two opposite placed vertices belong to the same phase, the resulting cut configuration is likewise ambiguous as seen in Figure 4. However, both these potential shortcomings can be alleviated by testing the material phase in the center of the volume spanned by the two potential phases, i.e. by evaluating the level set field at the appropriate location(s) and checking which phase it belongs to. Of course, in perfect arithmetic, the center point could be evaluated to be precisely zero, i.e. on the interface, and in such cases, the choice is indeed ambiguous. In this work we have chosen that such situations is assigned the solid phase, but it is worth noting that none of our numerical experiments have shown this to happen.

2.3 Implementation details

The level set and cut element method approach described in sections 2.1 and 2.2 are implemented as an extension to the open source framework for large-scale topology optimization (Aage et al., 2015) based on PETSc (Balay et al., 2018b,a, 1997). The major differences to the base code are: 1) the level set approach uses nodal based design variables, 2) a marching cubes algorithm is used to find the cut locations, 3) TetGen (Si, 2015) is employed for the sub-tetrahedralization and 4) the sub-element integration and the semi-discrete sensitivity evaluation, follows the approach presented in Andreasen et al. (2020).

The iterative solver used for this study has the same overall layout as the one presented in Aage et al. (2015), i.e. a multigrid preconditioner Krylov method. This is intentional since part of the aim of this work is to investigate how well solution methods originally developed for density methods perform for a large-scale crisp interface level set method, including the iterative solvers. However, some notable modifications have been made, partly due to the addition of new Krylov methods within the PETSc library and partly due to experiences made since 2015. First, the outer Krylov solver is changed to a flexible conjugate gradient (FCG) method as this is now available within PETSc and because it uses less memory than the flexible generalized minimum residual (FGMRES) method. Note that the flexible method is needed in either case since the preconditioner changes with the input vector, i.e. it is slightly varying. The preconditioner is a V-cycle multigrid method in which the smoothing steps are performed by four sweeps of a local SOR preconditioned Chebyshev method and where the coarse grid correction is obtained by an AMG preconditioned GMRES method. The change in smoothing and coarse grid correction is adopted from Aage et al. (2017), as this combination was found to have superior performance compared to the default settings in the GitHub code. The

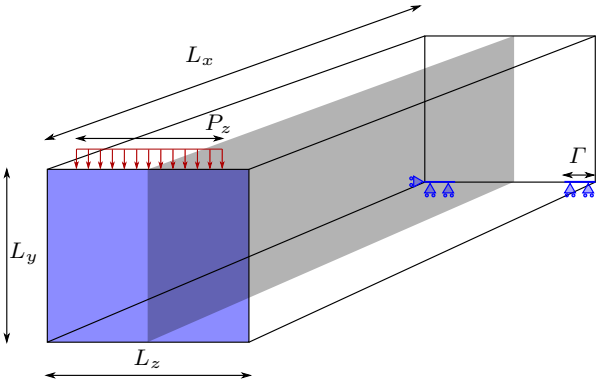

Fig. 5: Modeling domain for the MBB design problem with dimensions $L_x = 3$, $L_y = 1$ and $L_z = 1.25$, symmetry boundary condition on the front wall, simply supported at the two blue lines with length $\Gamma = 0.25$ and loaded by a downward line load with length $P_z = 1$ and nodal magnitude 0.1. The gray wall indicate a symmetry plane for the design variables.

linear systems are solved to a relative tolerance of $||\mathbf{Ku}-\mathbf{f}||/||\mathbf{f}|| < 10^{-6}$.

3 Numerical examples

All numerical experiments are performed on the DTU cluster Sophia consisting of 555 compute nodes each with 2 AMD EPYC 7351 16 core processors and 128 GB RAM memory. The aim of the numerical experiments is to demonstrate the length scale capabilities and the large-scale modeling capabilities of the proposed design formulation.

The MMA parameters and outer move limits are as described in Andreasen et al. (2020) except for the MMA constraint penalization parameter, c. In this work, the initial objective function is scaled such that $\Phi_0 = 5$ and the MMA penalization parameter is initialized to a low number, i.e. $c = 10$. This ensures that the volume constraint does not dominate the optimization process. This is especially necessary if the initial configuration violates the target volume fraction. The penalty parameter is then updated every 20th iteration as $c = 1.05c$ until the volume constraint is feasible. Note that for all numerical examples investigated in this work, the penalty parameter never exceeds $c = 25$.

Common for all the numerical examples is the use of isotropic material with $E_0 = 100$ and $\nu = 0.3$.

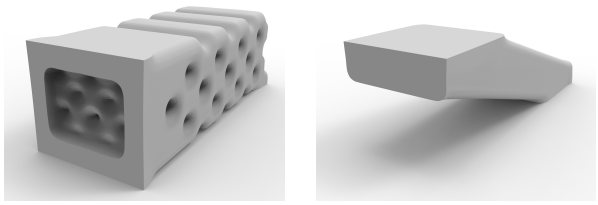

(a) (b)

Fig. 6: Initial configurations for the MBB design problem visualized using a mesh of $192 \times 64 \times 80$ elements.

3.1 MBB problem

The first numerical example concerns the classical MBB half-beam as seen in Figure 5 where dimensions, loads and supports are defined. The simulation is conducted on the full modeling domain while a symmetry plane has been introduced to explicitly enforce symmetry in the optimized designs. This alleviates potential length scale violations due to the filter Neumann condition on the gray symmetry plane. We remark that no length scale violations has been observed along the blue plane, and hence, no special treatment is given here. We remark that an alternative to the explicit enforcement of design symmetry would be to use a PDE-filter (Lazarov and Sigmund, 2011) and apply Robin conditions(Wallin et al., 2020). The target volume fraction is set to $V^b_{\text{target}} = 0.06$ and a filter radius of $R = 0.125$ corresponding to 8 element side lengths is applied. The problem is solved for the following four projection offsets $\Delta\eta = \{0, 0.01, 0.1, 0.2\}$.

3.1.1 Length scale control

First, the optimization process is started with the initial configuration seen in Figure 6(a) which is noted to heavily violate the volume constraint. The initial volume fraction is computed to be $V^b_0(\mathbf{s}) = 0.39$ and thus significantly above the target of 0.06. This reveals an intrinsic problem with most level set methods, i.e. that creating feasible initial configurations poses a significant challenge compared to density methods. This issue is especially pronounced in the low volume fraction limit, which is often encountered in three dimensional problems. This issue is the main motivation for the proposed MMA c-update scheme. But even with the proposed penalty parameter update scheme, starting infeasible is difficult and comes at the price of an increase in the number of design iterations. Partly due to this additional cost and partly because all example problems are solved in less than 10 hours, the optimization

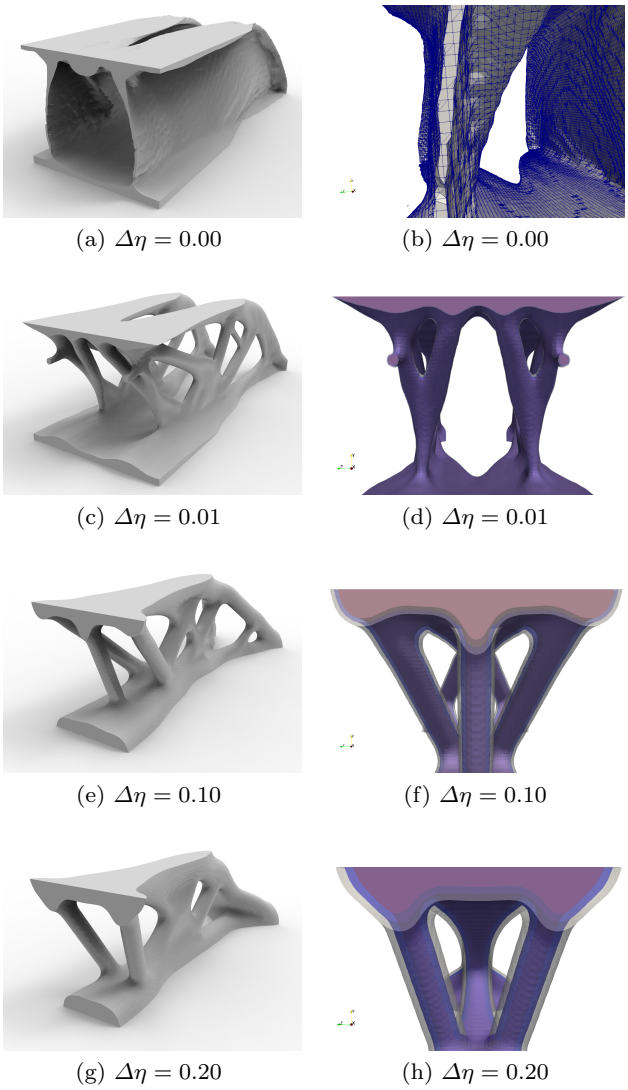

(a) $\Delta\eta = 0.00$ (b) $\Delta\eta = 0.00$

(c) $\Delta\eta = 0.01$ (d) $\Delta\eta = 0.01$

(e) $\Delta\eta = 0.10$ (f) $\Delta\eta = 0.10$

(g) $\Delta\eta = 0.20$ (h) $\Delta\eta = 0.20$

Fig. 7: Optimized MBB beams on a mesh with $192 \times 64 \times 80$ elements solved for different projection offsets. The final objective function values are: $\Phi_{\Delta\eta=0.00} = 171$, $\Phi_{\Delta\eta=0.01} = 201$, $\Phi_{\Delta\eta=0.10} = 276$ and $\Phi_{\Delta\eta=0.20} = 357$.

process is set to run for a fixed number of iterations, namely 600 design cycles.

The first set of optimized designs are computed on a mesh of $192 \times 64 \times 80$ (∼one million) elements and were obtained in 90 minutes using 64 cores. The blueprint realizations can be seen in the left column of Figure 7 where the projection offset is increased from top to bottom. The design in Figure 7(a) was obtained using $\Delta\eta = 0$, i.e. without an imposed length scale. The resulting design is seen to consist of two vertical closed walls connecting a top and a bottom plate, i.e. a double I-profile. This is exactly as expected since the best theoretical stiffness design is known to consist of in-

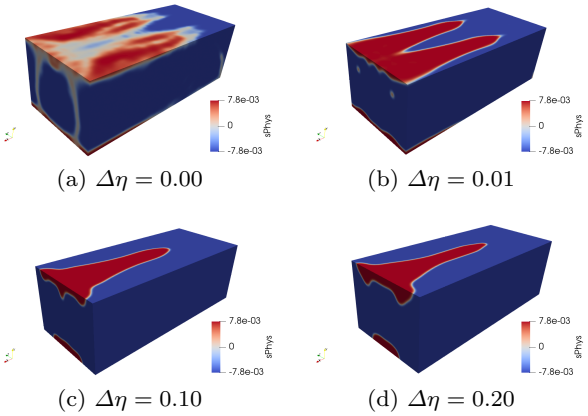

(a) $\Delta\eta = 0.00$ (b) $\Delta\eta = 0.01$

(c) $\Delta\eta = 0.10$ (d) $\Delta\eta = 0.20$

Fig. 8: Surface plots of the final physical level set fields for the designs in Figure 7, demonstrating that the robust approach ensures the lower and upper bound are met.

finitely thin closed walls (Michell, 1904). However, due to the finite size introduced by the underlying mesh, the walls cannot be infinitely thin and by inspection of the zoom-in plot in Figure 7(b) it is clear that the wall thickness is limited to being approximately one element thick, and even thinner at places. This of course means that the solution will be highly mesh dependent, but more importantly also that the physical model is of very poor quality. Hence, there is a real and present need for length scale control to ensure that the optimizer does not utilize poor numerical modeling to achieve good objective values. From a practical perspective length scale control is needed due to manufacturing limitations and it is therefore crucial if a proposed design tool should have any industrial relevance.

The remaining optimized design in Figure 7(c,e,g) are solved using an increasing projection offset, and by visual inspection it is clear that as $\Delta\eta$ is increased, the design complexity decreases and the imposed length scale becomes larger. Figure 7(d,f,h) shows the three realizations colored such that red/violet refers to eroded, blue to blueprint and gray to the dilated design. From these plots it is evident that the robust approach performs as observed in density methods, meaning that the separation between the three realizations remain constant and depends solely on the size of the projection offset. It is also noted that the objective values increase as the imposed length scale becomes larger which, again, is in perfect agreement with theoretical predictions (Sigmund et al., 2016).

Contrary to density methods, a crisp interface level set method does not care which values the level set field assume inside the solid and void regions, as long

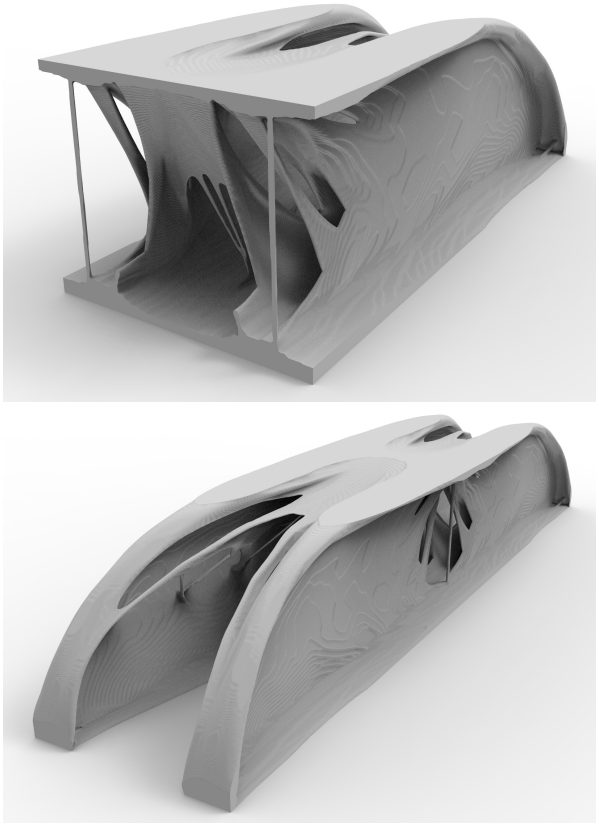

Fig. 9: Optimized MBB beams on a mesh of $768 \times 256 \times 320$ elements with a projection offset of $\Delta\eta = 0.01$ and final objective of $\Phi_{\Delta\eta=0.01} = 3021$ initialized with the design in Figure 6(a)

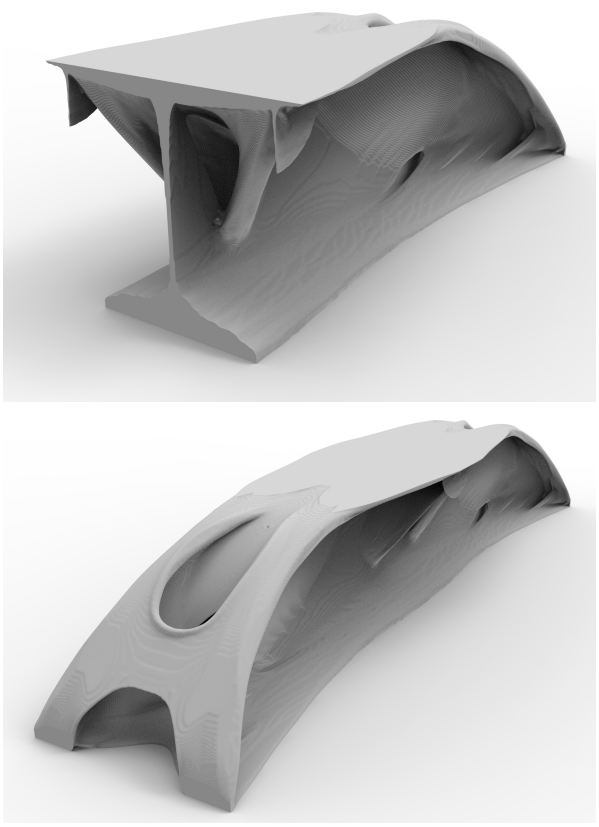

Fig. 10: Optimized MBB beams on a mesh with $768 \times 256 \times 320$ elements with a projection offset of $\Delta\eta = 0.01$ and final objective of $\Phi_{\Delta\eta=0.01} = 3230$ initialized with the design in Figure 6(b)

as $\bar{\tilde{s}}_i > 0$ or $\bar{\tilde{s}}_i < 0$, respectively. However, the robust approach utilized here to control the length scale relies on a well-defined gradient in the filtered field for the subsequent projection to be meaningful. This can only be ensured if the underling density field has reached either the upper or the lower bound in the entirety of the domain. This makes it interesting to investigate the physical level set fields in their continuous form, which is visualized in Figure 8 for the four designs from Figure 7. The problem solved without a projection threshold is seen in Figure 8(a), which shows large areas of $\bar{\tilde{s}}_i$ that does not meet the upper and lower bound despite the application of the threshold projection. This means that the gradient of this level set field has little use for controlling the length scale or for measuring the perimeter, which is an often used tool in level set methods. Many previous works address this issue by re-initializing the level set field to a signed distance field. Although this approach works, it comes at the cost of having to solve (at least partially) an auxiliary partial differential equation. However, when introducing a non-zero projection offset, the level set field is seen to take on either the lower or upper bound and thus providing the necessary well-defined gradient. This can be seen in Figure 8(b-d) where the gray area between red and blue defines the gradient. It is noted that the uniformity of the gradient is increased with increasing projection offset, i.e. the gray boundary is sharper defined in Figure 8(d) than seen in Figure 8(b).

3.1.2 Numerical performance

Having established that the proposed level set method enables length scale control, the next step is to investigate its large-scale capabilities. In order to make this test as challenging as possible, the imposed length scale is set to a bare minimum such that it only prohibits sub-element sized features. This is chosen, as the multigrid preconditioned iterative solver is known to be most challenged for high contrast problems with an additional high degree of heterogeneity, i.e. when small features are present (Aage et al., 2017). The specific filter parameters are $\Delta\eta = 0.01$, $R = 0.019$ and the

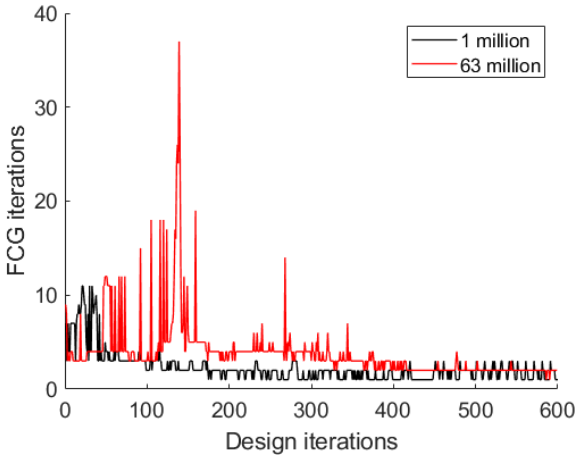

Fig. 11: Number of FCG iterations per design cycle for the high and low resolution optimized designs in Figure 9 and 7(c), respectively.

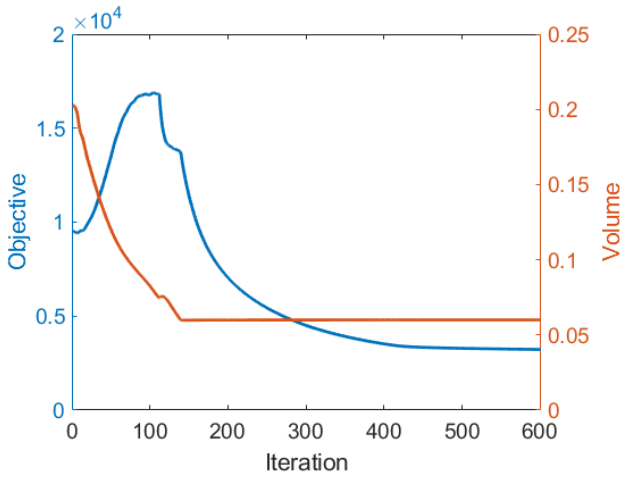

Fig. 12: Evolution of the objective function and blueprint volume for the optimized design in Figure 10 for a target volume of $V^b_{\text{target}} = 0.06$.

target volume is set to $V^b_{\text{target}} = 0.06$. The MBB problem is solved on a mesh of $768 \times 256 \times 320$ (∼63 million) elements using 800 cores. This leads to a design cycle time of approximately 60 seconds meaning that the 600 iterations are reached after 10 hours. The resulting optimized designs are shown in Figure 9 and Figure 10 using the initial configurations shown in Figure 6(a) and (b), respectively. First, it is noted that the final design is highly dependent on the initial configuration. This is a commonly known issue with level set methods and is due to the design only being able to evolve from the surface. As expected, we also find the lowest objective function for the design initialized using a configuration with holes. However, it is worth noting that three dimensional level set methods can introduce holes, i.e. that there is no need for hole nucleation schemes as needed in two dimensions. This is most clearly seen from the design in Figure 10 which was initialized using as the solid beam from Figure 6(b). The design in Figure 9 contains two vertical plate-like areas and several thin members emanating from the many initial holes while the design in Figure 10 contains less thin members and has a single vertical plate structure in the center part of the beam while it is branching towards the supports. The performance of the very detailed design is approx. 6% better.

Returning the discussion to the large-scale capabilities and the performance of the multigrid based Krylov solver, Figure 11 shows the number of FCG iterations as function of design cycles. The figure includes both the 63 million element example from Figure 9 and the 1 million element example from Figure 7(c). The plots reveal two main characteristics. First, it is seen that the maximum and average number of iterations are 11 and 2.3 for the one million elements design and 37 and 3.9 for the 63 million elements design, respectively. These observations are, as expected, in good agreement with previous reports on the same type of preconditioners applied to density based topology optimization problems(Amir et al., 2014; Aage et al., 2015, 2017; Baandrup et al., 2020). Secondly, it is observed that both design processes ends up using less than three FCG iterations for the last 200 design cycles. This implies that additional speed-up could be achieved through preconditioner re-usage. Comparing the finite element solver performance of the presented level set method to the freely available density method on GitHub reveals the following observations. First, the initial state problem is considerably more expensive to solve than what is the case for the density approach. This is attributed to the fact that the level set method always operates with crisp 0-1 solutions whereas the density code starts with a uniform material distribution. This is as expected due to the increased heterogeneity for the non-uniform starting guess used for a level set method. Based on our numerical experiments, the first iteration can take up to 4 times the number of Krylov iterations compared to the density code. This increase in solver cycles is, however, quickly reduced to a level comparable to the density method, and from around iteration 200, the two methods lead to equal solver performance. Secondly, although the solution to the finite element problem is responsible for more than 95% of the total run time for all problems considered here, the additional tasks of determining cut locations and the special integration of the cut elements, also means a deterioration in performance when compared to the density method. However,

it is worth noting that for increasing mesh resolution, the cut element specific operations takes up a smaller percentage of the total computational burden. The explanation of this is due to the following main reason. The best parallel performance is obtained by keeping the number of elements per process more or less fixed when increasing the mesh resolution, i.e. only the number of MPI tasks is increased. Since all cut operations are purely local, the amount of time spend on this remains constant. This is, however, not the case for the iterative solver where the construction, as well as application, of the preconditioner becomes more expensive. Moreover, as the linear system grows in size, the number of iterations needed to reach an acceptable solution also increases which is evident from Figure 11. Hence, for high resolution problems the difference in numerical performance between the density method and the cut element level set method is drastically reduced. This is an interesting observation since these findings are in stark contrast to the observations made for the 2D study in Andreasen et al. (2020) using Matlab. There it was found that the density method was significantly faster than the level set approach. Besides the parallelization aspect described above, this can be further explained by the fact that the 2D Matlab code was coded easily readable without significant use of vectorization. A further difference in the behavior of the optimizer and the number of iterations needed may be associated to the design evolution of a 3D level set field which is more free and therefore faster than 2D, e.g. holes can form from the sides.

The numerical experiment concerning the MBB beam is concluded with an inspection of the history for both objective and volume constraint as seen in Figure 12 for the design in Figure 10. The history plot clearly exemplify the issue with an infeasible starting configuration, meaning that the first 150 cycles are spent on reaching the target volume. However, from additional unreported studies initialized using a thin beam with feasible volume constraint it has been observed that many design iterations are spent evolving the design and creating holes while not achieving better final objective value despite being feasible initially. The plot also shows that the evolution of the objective function is smooth and that the objective value does not change much during the last 200 cycles. This is in good accordance with the observation regarding the number of FCG iterations needed during this phase of the optimization process.

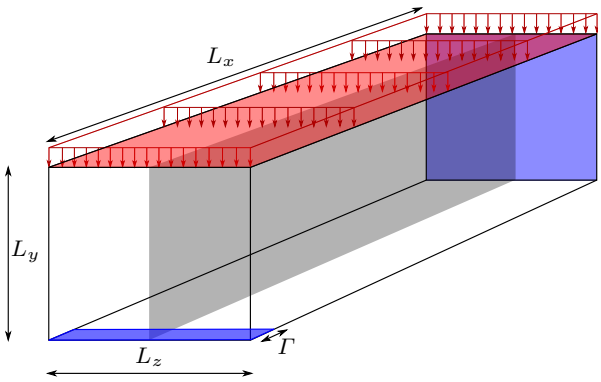

Fig. 13: Modeling domain for the bridge design problem with dimensions $L_x = 3$, $L_y = 1$ and $L_z = 1.25$, symmetry boundary condition on the back wall, fixed supports in the blue rectangle where $\Gamma = 0.25$ and loaded by a uniform pressure load with magnitude 1. The gray wall indicate a symmetry plane for the design variables.

3.2 Bridge problem

The numerical experiment section is concluded with a bridge design problem as shown in Figure 13. This example is especially interesting when seen from a length scale perspective as the distributed loading invites for more structural details compared to single load problems which often leads to closed wall structures as shown in the previous section. The bridge problem is solved on a mesh $768 \times 256 \times 320$ ($\sim$63 million) elements using 800 cores, a filter radius $R = 0.019$ and a target volume of $V^b_{\text{target}} = 0.12$. To ensure a well-defined structure where the load is applied, the top layer of nodes are considered passive solid and excluded from the set of optimization variables. This also means the nodes are excluded from the projection filter. Similarly, as for the MBB design problem, an additional symmetry plane is included, and hence, only half of the nodes in the computational domain are active design variables. The optimization process is started using the initial configuration in Figure 14 where all nodes connected to load and boundary conditions are solid phase. The problem is solved for three different projection offsets, i.e $\Delta\eta = \{0.01, 0.1, 0.2\}$. The resulting optimized designs are shown in Figure 15 and each of them was obtained in approximately 10 hours. Visual inspection of the optimized designs reveal yet again that the proposed level set method is capable of producing designs with a clear separation of length scales dependent on the size of the chosen $\Delta\eta$. Keeping in mind that all three cases are started from the same initial configuration it also evident that considerable

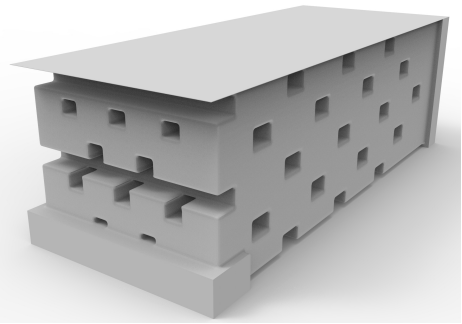

Fig. 14: Initial configuration used for the bridge design problem. The top layer of nodes, where the load is applied, are set as passive solid.

topological changes are achieved throughout the course of the optimization process, and thus, that the proposed level set method is indeed a topology optimization approach. In the small length scale design (Figure 15(a)) a very finely branched support structure is observed near the bridge deck while for larger length scales (Figure 15(b-c)) the support structure is increasingly solid and contain plate-like features.

By inspection of the objective function values for the bridge design examples it is noted that the length scale has the expected effect on the stiffness performance, i.e. decreasing stiffness with increasing length scale.

4 Discussion

In this work, we have presented a high resolution three dimensional level set topology optimization approach with length scale control. The approach is based on methods originally developed for density methods, where the major difference lies in the finite element analysis and the sensitivities calculation, which are obtained using a crisp interface cut element method. Through numerical experiments we have shown that the proposed approach is capable of enforcing and controlling the minimum length scale of the optimized designs by application of a projection filter using a constant steepness parameter of $\beta = 12$. Furthermore, we have demonstrated that high-resolution designs using high performance computing is possible and that the performance of the state solver, i.e. a domain decomposition multigrid preconditioned Krylov method, performs similar to that seen for the density method, for which it was originally developed. Moreover, the current implementation was based on an open-source framework for density based topology optimization and this work goes to prove that it is "easy" to modify or extend a density method to become a crisp interface level set approach.

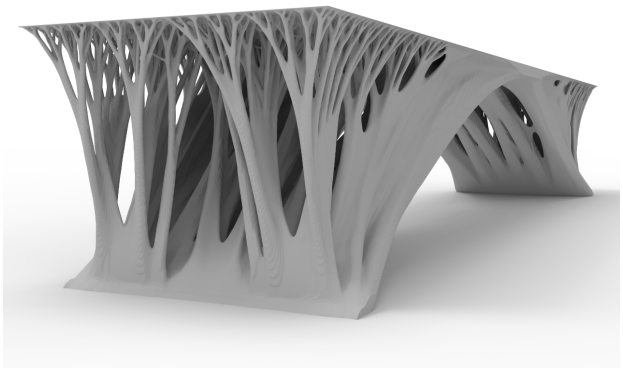

(a) $\Delta\eta = 0.01$ and $\Phi_{\Delta\eta=0.01} = 2.70 \cdot 10^8$

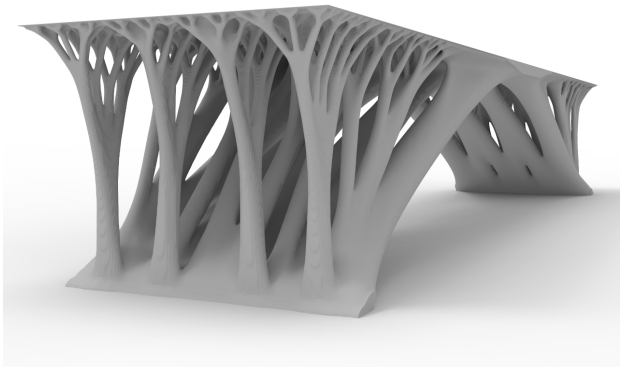

(b) $\Delta\eta = 0.10$ and $\Phi_{\Delta\eta=0.10} = 2.90 \cdot 10^8$

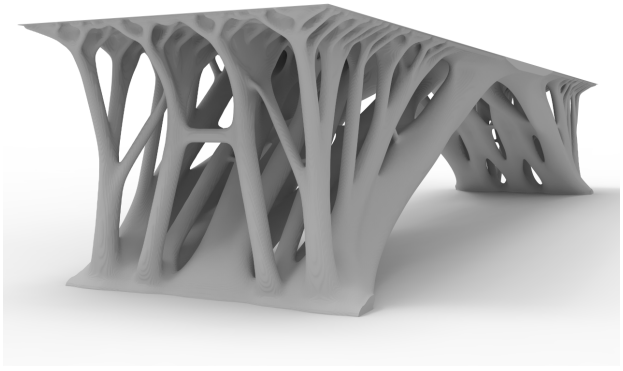

(c) $\Delta\eta = 0.20$ and $\Phi_{\Delta\eta=0.20} = 3.20 \cdot 10^8$

Fig. 15: Optimized bridge designs using a mesh of $768 \times 256 \times 320$ elements solved for different projection offsets.

It is worth noting that the length scale control method employed in this work, i.e. the robust design formalism, has a number of potential drawbacks. For example, the simplified version where only a single finite element analysis is performed on the eroded design, does not work for general optimization problems. For most other problems than the minimum compliance with a volume constraint, finite element analyses is required for *all* considered realizations. Hence, a minimum of two finite element analyses is needed to impose a minimum length scale. Since more than 95% of the compute time is spent on the linear solution of the finite element problem, this will approximately increase the total CPU time with a multiple of the used number of realizations. However, if computational resources are not a concern, one may use e.g. `MPI_Comm_split()` to solve each finite element analysis simultaneous and thus keep the wall clock time constant. This is not the case for the purely geometric constraint of e.g. Zhou et al. (2015). However, such constraints does not ensure that the performance of the optimized design is maintained if too much, or too little, material is removed/added during fabrication, since only the blueprint design is analyzed by finite elements. In many cases, this is not acceptable from a practical perspective. On the other hand, when the robust design method is applied to stress constraint problems it is possible to ensure the allowed stress target is not violated for a considerable interval of over/under machining, see da Silva et al. (2019, 2020) for more discussion. This would not be achievable with the pure geometric constraints.

The numerical experiments also showed that the proposed level set method is sensitive to the initial configuration, which is a commonly known problem for boundary evolution design methods. However, it was also found that from any given initial configuration the best performing design is always the one with the lowest projection offset and that the performance deteriorates with increasing $\Delta\eta$. Thus, despite the level set approach being highly susceptible to local minima, the length scale control scheme works exactly as expected.

Special attention was given to the low volume fraction limit and a simple update rule for the MMA penalty parameter was proposed to allow for starting with initial designs that heavily violates the volume constraint, while at the same time giving proper weight to the objective function.

Several open questions remain and should be investigated in future works. This includes a robust approach to generate feasible initial configurations in the low volume fraction limit. Surely, this could be achieved using the density method, but an elegant and robust approach that does not depend on solving an additional optimization problem is desirable as the challenge grows with increasing complexity of constraints e.g. stress constraints. Finally, and maybe more importantly, one may argue that there are better design problems to be solved using a crisp interface level set method than the minimum compliance problem. That is, problems involving interface conditions such as multiphysics problems. In that relation, it is worth mentioning that the proposed cut element based level set design methodology recently has been successfully applied to fully coupled vibroacoustic shape optimization in two dimensions (Dilgen and Aage, 2021).

Acknowledgements The authors would like to thank the Villum Foundation for the funding of the Villum Investigator grant through the InnoTop project.

Conflict of interest

The authors declare that they have no conflict of interest.

Replication of results

All the details necessary to reproduce the results in Section 3 have been defined in the paper. The interested reader may contact the corresponding author for further implementation details.

Supplementary material

STL files of the three optimized bridge designs from Figure 15 are available from DOI: `10.11583/DTU.c.5326625`

References

Aage N, Lazarov BS (2013) Parallel framework for topology optimization using the method of moving asymptotes. Struct Multidiscip Optim 47(4):493–505, DOI 10.1007/s00158-012-0869-2

Aage N, Andreassen E, Lazarov BS (2015) Topology optimization using PETSc: An easy-to-use, fully parallel, open source topology optimization framework. Struct Multidiscip Optim 51(3):565–572, DOI 10.1007/s00158-014-1157-0

Aage N, Andreassen E, Lazarov BS, Sigmund O (2017) Giga-voxel computational morphogenesis for structural design. Nature 550(7674):84–86, DOI 10.1038/nature23911

Amir O, Aage N, Lazarov BS (2014) On multigrid-CG for efficient topology optimization. Struct Multidiscip Optim 49(5):815–829, DOI 10.1007/s00158-013-1015-5

Andreasen CS, Elingaard MO, Aage N (2020) Level set topology and shape optimization by density methods using cut elements with length scale control. Struct Multidiscip Optim 62(2):685–707, DOI 10.1007/s00158-020-02527-1

Baandrup M, Sigmund O, Polk H, Aage N (2020) Closing the gap towards super-long suspension bridges using computational morphogenesis. Nat Commun 11(1):2735, DOI 10.1038/s41467-020-16599-6

Balay S, Gropp WD, McInnes LC, Smith BF (1997) Efficient Management of Parallelism in Object Oriented Numerical Software Libraries. In: Arge E, Bruaset AM, Langtangen HP (eds) Mod. Softw. Tools Sci. Comput., Birkhäuser Press, pp 163–202

Balay S, Abhyankar S, Adams M, Brown J, Brune P, Buschelman K, Dalcin L, Dener A, Eijkhout V, Gropp W, Kaushik D, Knepley M, May D, McInnes LC, Mills RT, Munson T, Rupp K, Sanan P, Smith B, Zampini S, Zhang H, Zhang H (2018a) {PETS}c Users Manual. Tech. Rep. ANL-95/11 - Revision 3.10, Argonne National Laboratory

Balay S, Abhyankar S, Adams M, Brown J, Brune P, Buschelman K, Dalcin L, Dener A, Eijkhout V, Gropp W, Kaushik D, Knepley M, May D, McInnes LC, Mills RT, Munson T, Rupp K, Sanan P, Smith B, Zampini S, Zhang H, Zhang H (2018b) {PETS}c {W}eb page. \url{http://www.mcs.anl.gov/petsc}

Barrera JL, Maute K (2020) Ambiguous phase assignment of discretized 3D geometries in topology optimization. Comput Methods Appl Mech Eng 369:113201, DOI 10.1016/j.cma.2020.113201, 2002.10255

Barrera JL, Geiss MJ, Maute K (2020) Hole seeding in level set topology optimization via density fields. Struct Multidiscip Optim 61(4):1319–1343, DOI 10.1007/s00158-019-02480-8, 1909.10703

Belytschko T, Black T (1999) Elastic crack growth in finite elements with minimal remeshing. Int J Numer Methods Eng 45(5):601–620, DOI 10.1002/(SICI)1097-0207(19990620)45:5⟨601::AID-NME598⟩3.0.CO;2-S

Bendsøe MP (1989) Optimal shape design as a material distribution problem. Struct Optim 1(4):193–202, DOI 10.1007/BF01650949

Bendsøe MP, Kikuchi N (1988) Generating optimal topologies in structural design using a homogenisation method. Comput Methods Appl Mech Eng 71(2):197–224

Bendsøe MP, Sigmund O (2004) Topology Optimization: Theory, Methods, and Applications. Engineering online library, Springer Berlin Heidelberg, Berlin, Heidelberg, DOI 10.1007/978-3-662-05086-6

Bourdin B (2001) Filters in topology optimization. Int J Numer Methods Eng 50(9):2143–2158, DOI 10.1002/nme.116

Burman E (2010) Ghost penalty. Comptes Rendus Math 348(21-22):1217–1220, DOI 10.1016/j.crma.2010.10.006

Chen S, Chen W (2011) A new level-set based approach to shape and topology optimization under geometric uncertainty. Struct Multidiscip Optim 44(1):1–18, DOI 10.1007/s00158-011-0660-9

Chen S, Wang MY, Liu AQ (2008) Shape feature control in structural topology optimization. Comput Des 40(9):951–962, DOI 10.1016/j.cad.2008.07.004

Chen S, Chen W, Lee S (2010) Level set based robust shape and topology optimization under random field uncertainties. Struct Multidiscip Optim 41(4):507–524, DOI 10.1007/s00158-009-0449-2

Christiansen RE, Lazarov BS, Jensen JS, Sigmund O (2015) Creating geometrically robust designs for highly sensitive problems using topology optimization: Acoustic cavity design. Struct Multidiscip Optim 52(4):737–754, DOI 10.1007/s00158-015-1265-5

Dapogny C, Dobrzynski C, Frey P (2014) Three-dimensional adaptive domain remeshing, implicit domain meshing, and applications to free and moving boundary problems. J Comput Phys 262:358–378, DOI 10.1016/j.jcp.2014.01.005

Dapogny C, Faure A, Michailidis G, Allaire G, Couvelas A, Estevez R (2017) Geometric constraints for shape and topology optimization in architectural design. Comput Mech 59(6):1–33, DOI 10.1007/s00466-017-1383-6

Dilgen CB, Aage N (2021) Generalized shape optimization of transient vibroacoustic problems using cut elements. Int J Numer Methods Eng p nme.6591, DOI 10.1002/nme.6591

Evgrafov A, Rupp CJ, Maute K, Dunn ML (2008) Large-scale parallel topology optimization using a dual-primal substructuring solver. Struct Multidiscip Optim 36:329–345, DOI 10.1007/s00158-007-0190-7

Feppon F, Allaire G, Dapogny C, Jolivet P (2020) Topology optimization of thermal fluid–structure systems using body-fitted meshes and parallel computing. J Comput Phys 417:109574, DOI 10.1016/j.jcp.2020.109574

Feppon F, Allaire G, Dapogny C, Jolivet P (2021) Body-fitted topology optimization of 2D and 3D fluid-to-fluid heat exchangers. Comput Methods Appl Mech Eng 376(August):113638, DOI 10.1016/j.

cma.2020.113638

Hansbo A, Hansbo P (2004) A finite element method for the simulation of strong and weak discontinuities in solid mechanics. Comput Methods Appl Mech Eng 193(33-35):3523–3540, DOI 10.1016/j.cma.2003.12.041

Jansen M (2019) Explicit level set and density methods for topology optimization with equivalent minimum length scale constraints. Struct Multidiscip Optim 59(5):1775–1788, DOI 10.1007/s00158-018-2162-5

Kambampati S, Jauregui C, Museth K, Kim HA (2020) Large-scale level set topology optimization for elasticity and heat conduction. Struct Multidiscip Optim 61(1):19–38, DOI 10.1007/s00158-019-02440-2

Lazarov BS, Sigmund O (2011) Filters in topology optimization based on Helmholtz-type differential equations. Int J Numer Methods Eng 86(6):765–781, DOI 10.1002/nme.3072

Liu H, Hu Y, Zhu B, Matusik W, Sifakis E (2019a) Narrow-band topology optimization on a sparsely populated grid. ACM Trans Graph 37(6):1–14, DOI 10.1145/3272127.3275012

Liu H, Tian Y, Zong H, Ma Q, Wang MY, Zhang L (2019b) Fully parallel level set method for large-scale structural topology optimization. Comput Struct 221(May):13–27, DOI 10.1016/j.compstruc.2019.05.010

Lorensen WE, Cline HE (1987) Marching Cubes: A High Resolution 3D Surface Construction Algorithm. SIGGRAPH Comput Graph 21(4):163–169, DOI 10.1145/37402.37422

Michell AGM (1904) Michell, A.G.M. 1904: The limits of economy of material in frame structures. 8,. PhilMag 8(47):589–597

Osher S, Sethian JA (1988) Fronts propagating with curvature-dependent speed: Algorithms based on Hamilton-Jacobi formulations. J Comput Phys 79(1):12–49, DOI 10.1016/0021-9991(88)90002-2, 9809069v1

de Prenter F, Verhoosel CV, van Brummelen EH, Evans JA, Messe C, Benzaken J, Maute K (2020) Multigrid solvers for immersed finite element methods and immersed isogeometric analysis. Comput Mech 65(3):807–838, DOI 10.1007/s00466-019-01796-y, 1903.10977

Sethian J, Wiegmann A (2000) Structural Boundary Design via Level Set and Immersed Interface Methods. J Comput Phys 163(2):489–528, DOI 10.1006/jcph.2000.6581, arXiv:1011.1669v3

Sharma A, Villanueva H, Maute K (2017) On shape sensitivities with heaviside-enriched XFEM. Struct Multidiscip Optim 55(2):385–408, DOI 10.1007/s00158-016-1640-x

Si H (2015) TetGen, a Delaunay-Based Quality Tetrahedral Mesh Generator. ACM Trans Math Softw 41(2), DOI 10.1145/2629697

Sigmund O, Maute K (2013) Topology optimization approaches. Struct Multidiscip Optim 48(6):1031–1055, DOI 10.1007/s00158-013-0978-6

Sigmund O, Aage N, Andreassen E (2016) On the (non-)optimality of Michell structures. Struct Multidiscip Optim 54(2):361–373, DOI 10.1007/s00158-016-1420-7

da Silva GA, Beck AT, Sigmund O (2019) Topology optimization of compliant mechanisms with stress constraints and manufacturing error robustness. Comput Methods Appl Mech Eng 354:397–421, DOI 10.1016/j.cma.2019.05.046

da Silva GA, Aage N, Beck AT, Sigmund O (2020) Three-dimensional manufacturing tolerant topology optimization with hundreds of millions of local stress constraints. Int J Numer Methods Eng p nme.6548, DOI 10.1002/nme.6548

Svanberg K (1987) The method of moving asymptotes - a new method for structural optimization. Int J Numer Methods Eng 24(June 1986):359–373, DOI 10.1002/nme.1620240207

Wallin M, Ivarsson N, Amir O, Tortorelli D (2020) Consistent boundary conditions for PDE filter regularization in topology optimization. Struct Multidiscip Optim DOI 10.1007/s00158-020-02556-w

Wang F, Lazarov BS, Sigmund O (2011) On projection methods, convergence and robust formulations in topology optimization. Struct Multidiscip Optim 43:767–784, DOI 10.1007/s00158-010-0602-y

Yamada T (2019) Thickness Constraints for Topology Optimization Using the Fictitious Physical Model. In: EngOpt 2018 Proc. 6th Int. Conf. Eng. Optim., Springer International Publishing, Cham, pp 483–490, DOI 10.1007/978-3-319-97773-7_43

Zhou M, Lazarov BS, Wang F, Sigmund O (2015) Minimum length scale in topology optimization by geometric constraints. Comput Methods Appl Mech Eng 293:266–282, DOI 10.1016/j.cma.2015.05.003